Electronic Supplementary Information

Experimental Section

Materials: Hydrochloric acid (HCl, 99.0%), ammonium chloride (NH_4Cl), ethanol (C_2H_6O, 99.0%), sodium hypochlorite solution (NaClO), triphenylphosphine (TPP) and graphite powder were purchased Aladdin Ltd. (Shanghai, China). Para-(dimethylamino) benzaldehyde ($C_9H_{11}NO$) and Nafion (5 wt%) solution was purchased from Sigma-Aldrich Chemical Reagent Co., Ltd. Hydrochloric acid, nitric acid, sulfuric acid, hydrogen peroxide and hydrazine monohydrate ($N_2H_4 \cdot H_2O$) were purchased from Beijing Chemical Corp. (China). chemical Ltd. in Chengdu. All chemical regents were used as received without further purification. Deionized water was made by the Millipore system and used in all experiments.

Synthesis of PG and G nanosheet: GO was prepared from graphite powder by a modified Hummers method.[1,2] PG was synthesized by thermal annealing of GO and triphenylphosphine (TPP). In a typical experiment, 100 mg of GO were mixed with 400 mg of TPP in 30 mL of ethanol at room temperature under stirring in an open beaker. After evaporation of ethanol, the obtained GO/TPP mixture was dried in a vacuum oven at 60 °C overnight. The annealing treatment was then carried out in a tube furnace with high purity argon as protective ambient. The resulting mixture was put in a quartz boat in the center of a tube furnace and annealed at the designed temperature (e.g., 1000 °C) for 1 h. The product was collected when the furnace temperature was below 60 °C. For comparison, PG with various atom percentages of P dopant (0.19 and 1.24 at%) was also prepared under the same condition. G

nanosheet was prepared under the same condition without the presence of TPP.

Characterizations: XRD data were collected on a Rigaku X-ray diffractometer equipped with a Cu Kα radiation source. Raman spectroscopy measurements were carried out on a Renishaw 1000 Raman imaging microscope system with an excitation wavelength of 632.8 nm. Transmission electron microscopy (TEM) images and energy dispersive X-ray (EDX) spectra were recorded on a FEI Tecnai T20. XPS measurements were performed on an ESCALABMK II X-ray photoelectron spectrometer using Mg as the exciting source. The absorbance data of spectrophotometer were acquired on SHIMADZU UV-1800 UV-Vis spectrophotometer. The ion chromatography data were collected on Thermofisher ICS 5000 plus using the dual temperature heater, injection valve, conductivity detector, AERS 500 Anions suppressor. The ion chromatography data were collected on Metrohm 940 Professional IC Vario.

Ion chromatography Details: Ion chromatographs are able to measure concentrations of major anions and cations. It measures concentrations of ionic species by separating them based on their interaction with a resin. Sample solutions pass through a pressurized chromatographic column where ions are absorbed by column constituents. In this work, liquid solutions, including of lithium and ammonium ions, should be filtered by chromatographic column covered by ion-exchange group ($-SO_3^-$), which can adsorb major cations, such as Li^+ and NH_4^+. As an ion extraction liquid (2mmol HNO_3) runs through the column, the absorbed ions begin separating from the column. The major cations, such as Li^+ and NH_4^+, have different ionic radius, and thus the

retention time of different species is distinct, which determines the ionic concentrations in the sample. The sample required for analysis is approximately 10 mL.

Electrochemical Measurements: N_2 reduction experiments were carried out in a two-compartment cell under ambient condition, which was separated by Nafion 117 membrane. The membrane was protonated by first boiling in ultrapure water for 1 h and treating in H_2O_2 (5 wt%) aqueous solution at 80 ℃ for another 1 h, respectively. And then, the membrane was treated in 0.5 M H_2SO_4 for 3 h at 80 ℃ and finally in water for 6 h. The electrochemical experiments were carried out with an electrochemical workstation (CHI 660E) using a three-electrode configuration with prepared electrodes, graphite rod, and Ag/AgCl electrode (saturated KCl electrolyte) as the working electrode, counter electrode, and reference electrode, respectively. The potentials reported in this work were converted to RHE scale via calibration with the following equation: E (vs RHE) = E (vs Ag/AgCl) + 0.059 × pH + 0.197 V and the presented current density was normalized to the geometric surface area. For electrochemical N_2 reduction, chronoamperometry tests were conducted in N_2-saturated 0.5 M $LiClO_4$ solution.

Determination of NH_3: The produced NH_3 was spectrophotometrically confirmed by the indophenol blue method.[3] Specifically, 4 mL electrolyte was obtained from the cathodic chamber and mixed with 50 μL oxidizing solution containing NaClO (p_{Cl} = 4 ~ 4.9) and NaOH (0.75 M), 500 μL coloring solution containing 0.4 M $C_7H_6O_3Na$ and 0.32 M NaOH, and 50 μL catalyst solution (1 wt% $Na_2[Fe(CN)_5NO]$) for 1 h.

Absorbance measurements were performed at 655 nm. The concentration-absorbance curve was calibrated using standard NH_3 solution with a series of concentrations. The fitting curve ($y = 0.519x + 0.016$, $R^2 = 0.998$) showed good linear relation of absorbance value with NH_3 concentration.

Determination of N_2H_4: The N_2H_4 possibly was estimated by the method of Watt and Chrisp.[4] A mixed solution of 1.97 g $C_9H_{11}NO$, 10 mL concentrated HCl, and 100 mL ethanol was used as a color reagent. Calibration curve was plotted as follows: first, preparing a series of N_2H_4 solutions of known concentration as standards; second, adding 4 mL color reagent to the above N_2H_4 solution, separately, and standing 20 min at room temperature; finally, the absorbance of the resulting solution was measured at 460 nm. The fitting curve showed good linear relation of absorbance with N_2H_4 concentration ($y = 1.02x + 0.072$, $R^2 = 0.998$).

Determination of FE and NH_3 Yield: The FE for N_2 reduction was defined as the amount of electric charge used for synthesizing NH_3 divided by the total charge passed through the electrodes during the electrolysis. The total amount of NH_3 produced was measured using colorimetric methods. Assuming three electrons were needed to produce one NH_3 molecule, the FE could be calculated as follows

$$FE = 3\times F\times[NH_3] \times V / (17 \times Q) \times 100\% \qquad (1)$$

NH_3 yield was calculated using the following equation

$$NH_3 \text{ yield} = [NH_3]\times V/(m_{cat.} \times t) \qquad (2)$$

where F is the Faraday constant, $[NH_3]$ is the measured NH_3 concentration, V is the

volume of the electrolyte in the cathodic chamber, Q is the total quantity of applied electricity; t is the reduction time; $m_{cat.}$ is the loaded mass of catalyst on carbon paper.

Computational Details: Spin-polarized DFT calculations were performed by using the plane wave-based Vienna ab initio simulation package (VASP).[5,6] The generalized gradient approximation method with Perdew-Burke-Ernzerhof (PBE) functional was used to describe the exchange-correlation interaction among electrons.[7] A hexagonal graphene supercell (6 × 6 graphene unit cell) containing 72 atoms with one of the C atoms substituted by a phosphorus atom is used to model the phosphorus doped grapheme, similar to that of Yang's work.[8] The van der Waals (vdW) correction with the Grimme approach (DFT-D3) was included in the interaction between single molecule/atoms and substrates.[9] The energy cutoff for the plane wave-basis expansion was set to 500 eV and the atomic relaxation was continued until the forces acting on atoms were smaller than 0.01 eV $Å^{-1}$. The Brillouin zone was sampled with 3 × 3 × 1 Gamma-center k-point mesh, and the electronic states were smeared using the Fermi scheme with a broadening width of 0.1 eV.

The free energies of the reaction intermediates were obtained by $\Delta G = \Delta E_{ads} + \Delta ZPE - T\Delta S + \Delta G(U) + \Delta G(pH)$, where ΔE_{ads} is the adsorption energy, ZPE is the zero point energy and S is the entropy at 298 K. The effect of a bias was included in calculating the free energy change of elementary reactions involving transfer of electrons by adding $\Delta G(U) = -neU$, where n is number of electrons transferred and U is the electrode potential.[10] In our calculations, we used U = –0.65 V (vs. RHE). $\Delta G(pH) = -k_B T \ln 10 \times pH$, where k_B is the Boltzmann constant, and pH = 7 for

electrolyte. In this study, the entropies of molecules in the gas phase are obtained from the literature.[11]

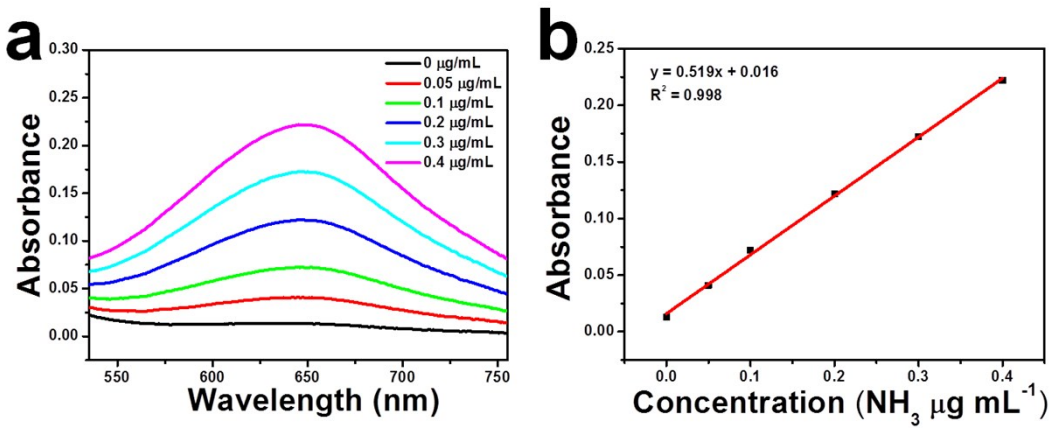

Fig. S1. (a) UV-vis absorption spectra of indophenol assays with NH_3 concentrations after incubated for 2 h at room temperature. (b) Calibration curve used for estimation of NH_3 concentration.

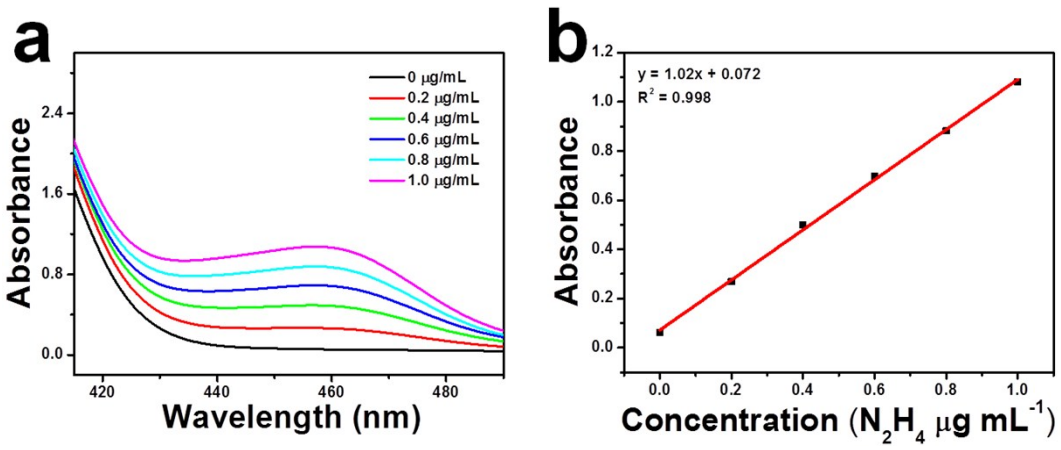

Fig. S2. (a) UV-vis absorption spectra of various N_2H_4 concentrations after incubated for 10 min at room temperature. (b) Calibration curve used for calculation of N_2H_4 concentration.

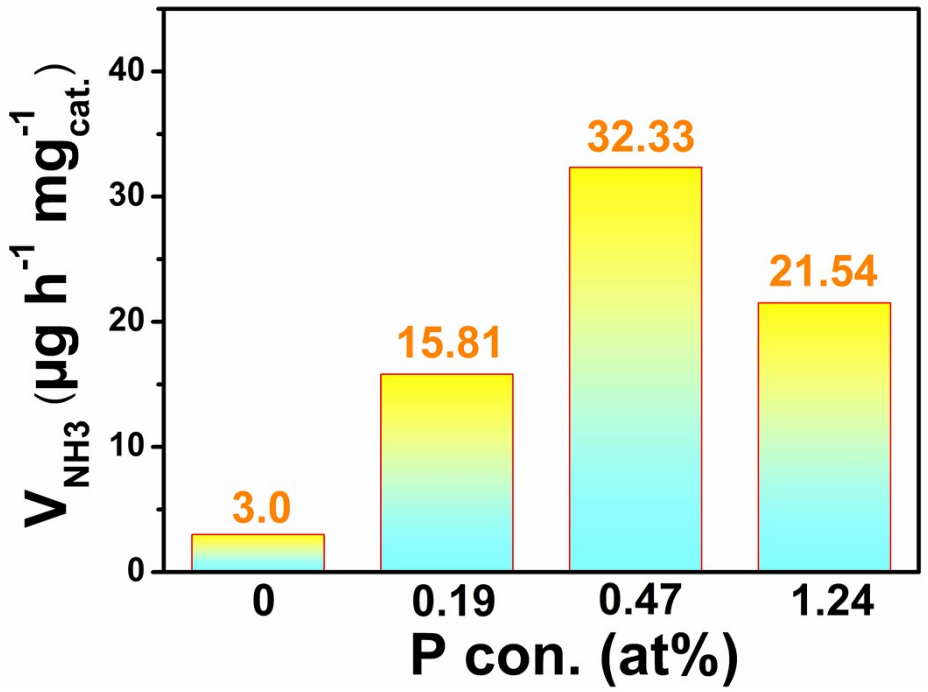

Fig. S3. The relationship between P dopant content and NH_3 yield at −0.65 V.

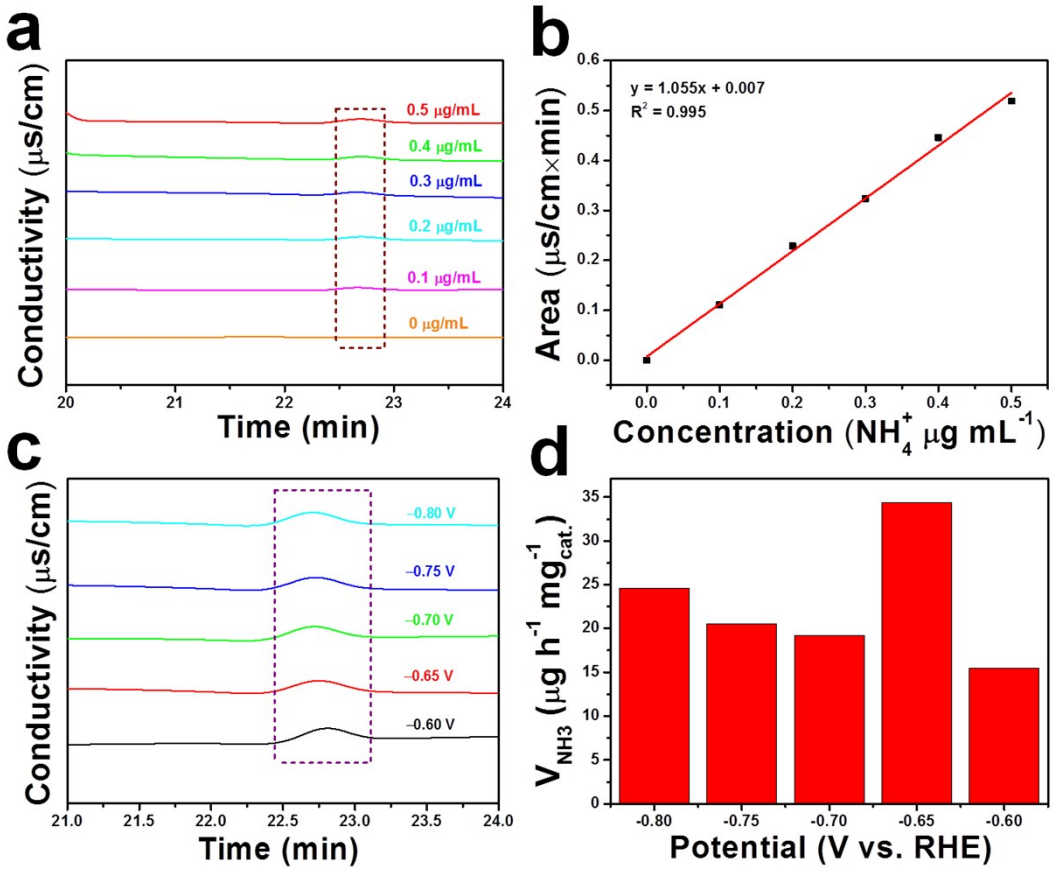

Fig. S4. (a) Ion chromatogram analysis for the NH_4^+ ions. (b) Calibration curve used for estimation of NH_4^+. (c) Ion chromatogram for the electrolytes at a series of potentials after electrolysis for 2 h. (d) V_{NH3} for PG/CP at corresponding potentials.

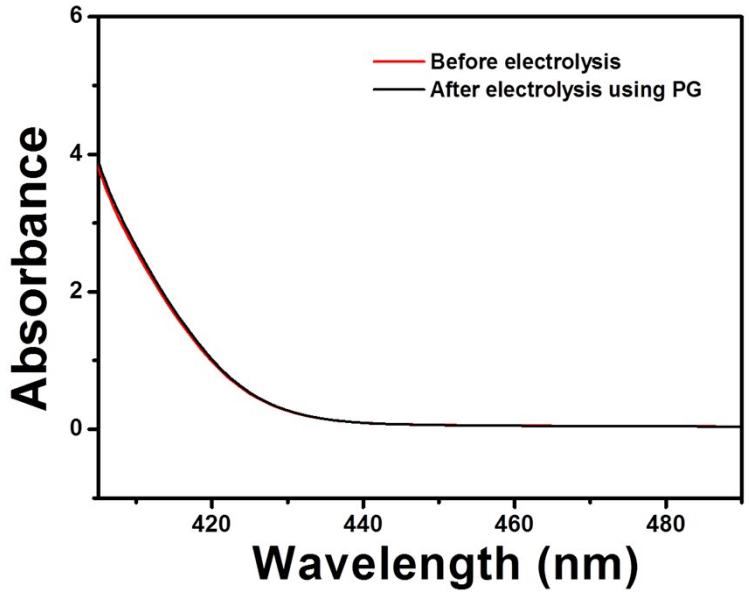

Fig. S5. UV-vis absorption spectra of the electrolytes estimated by the method of Watt and Chrisp before and after 2 h electrolysis in N_2 atmosphere at –0.65 V.

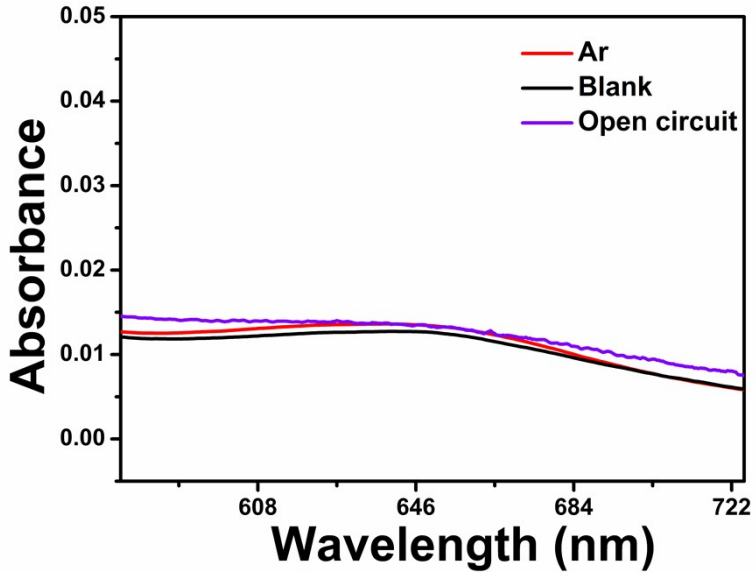

Fig. S6. UV-vis absorption spectra of the electrolytes stained with indophenol indicator after 2 h electrolysis in Ar-saturated solution at –0.65 V and N_2-saturated solution under open circuit potential.

.

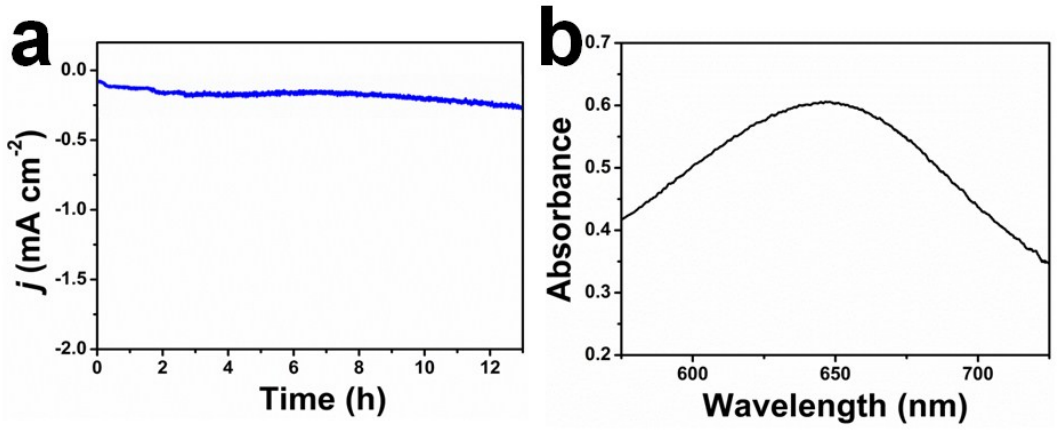

Fig. S7. (a) Time-dependent current density curve of PG/CP at −0.65 V after 13 h electrolysis and (b) corresponding UV-vis absorption spectrum of the electrolytes stained with indophenol indicator.

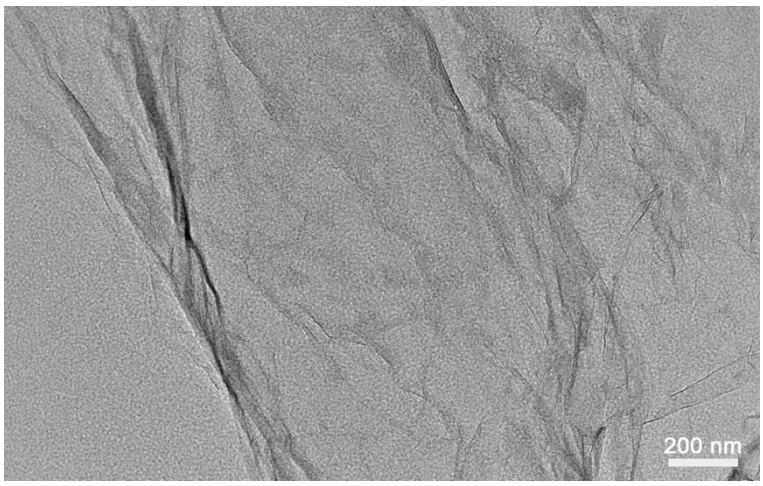

Fig. S8. TEM image of PG after long-term electrolysis

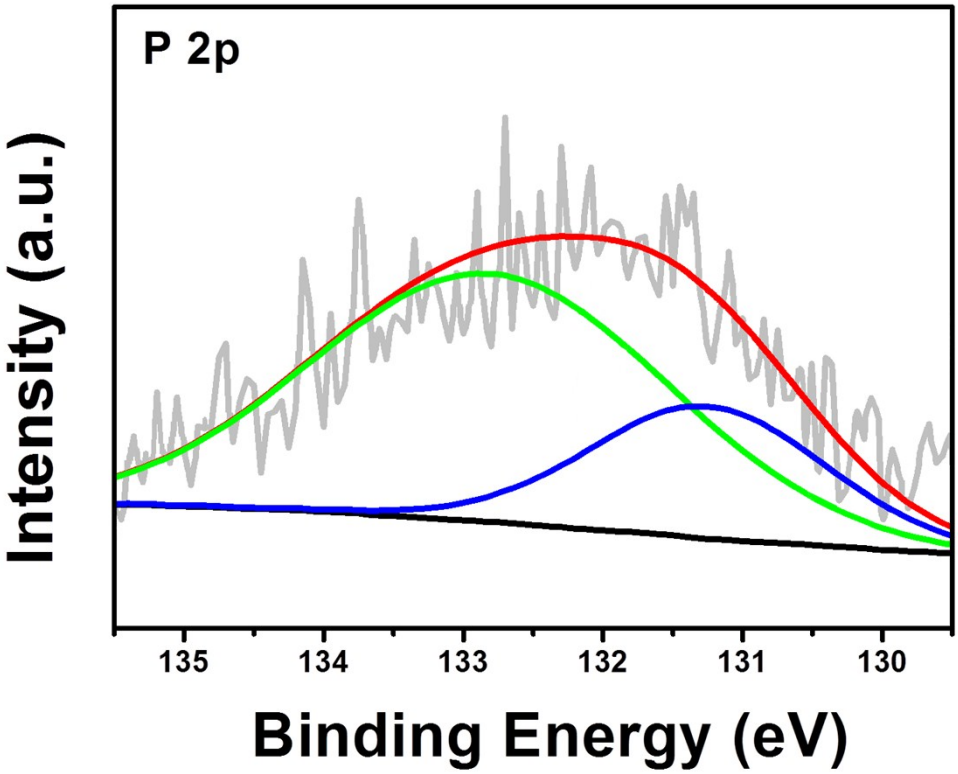

Fig. S9. XPS spectrum of PG in P 2p region after stability test.

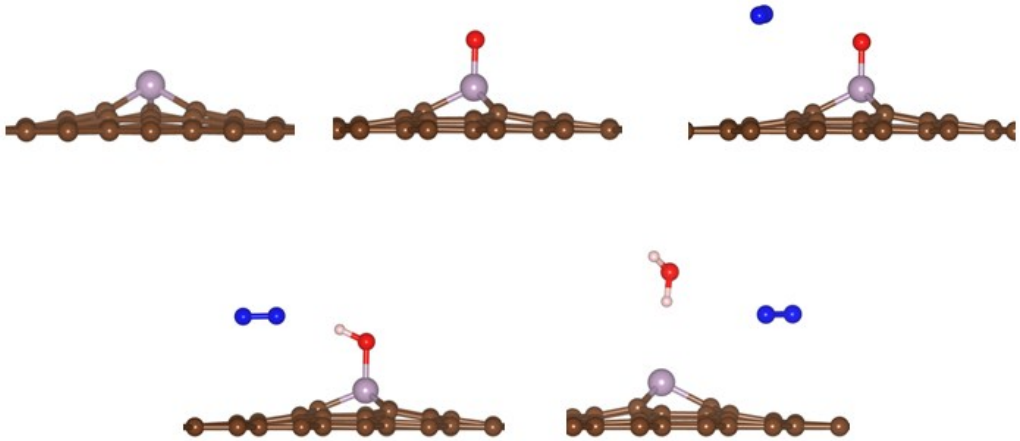

Fig. S10. The NRR on PG catalyst with P-O bonding. [Legend: brown, C; purple, P; blue, N; white, H; red, O.]

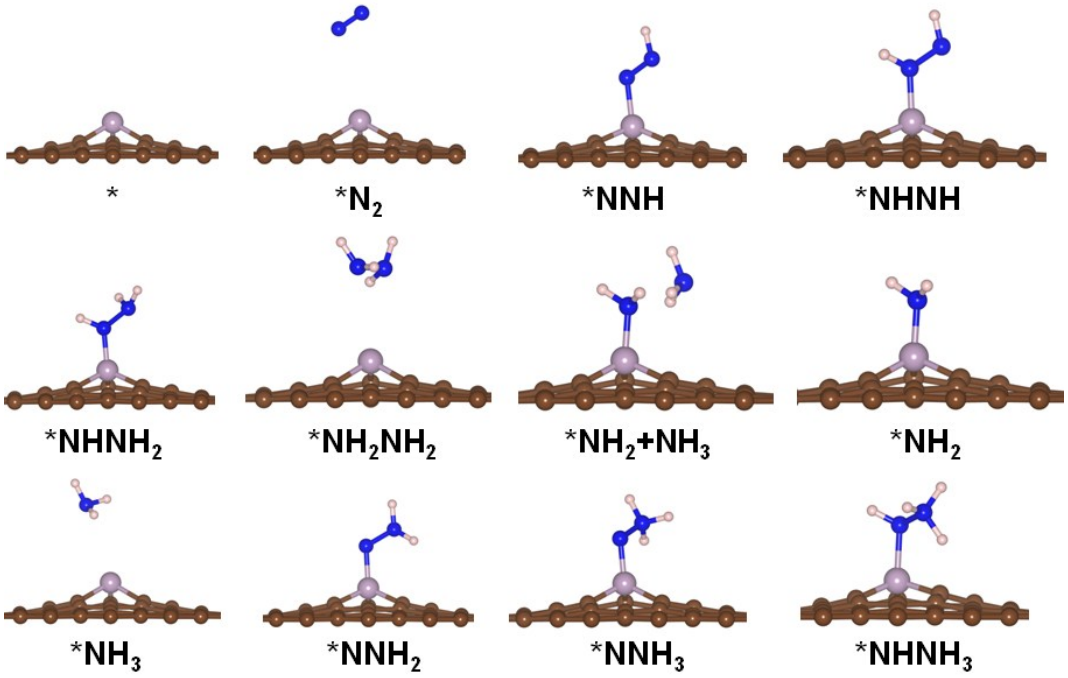

Fig. S11. Atom configurations for NRR on PG catalyst.

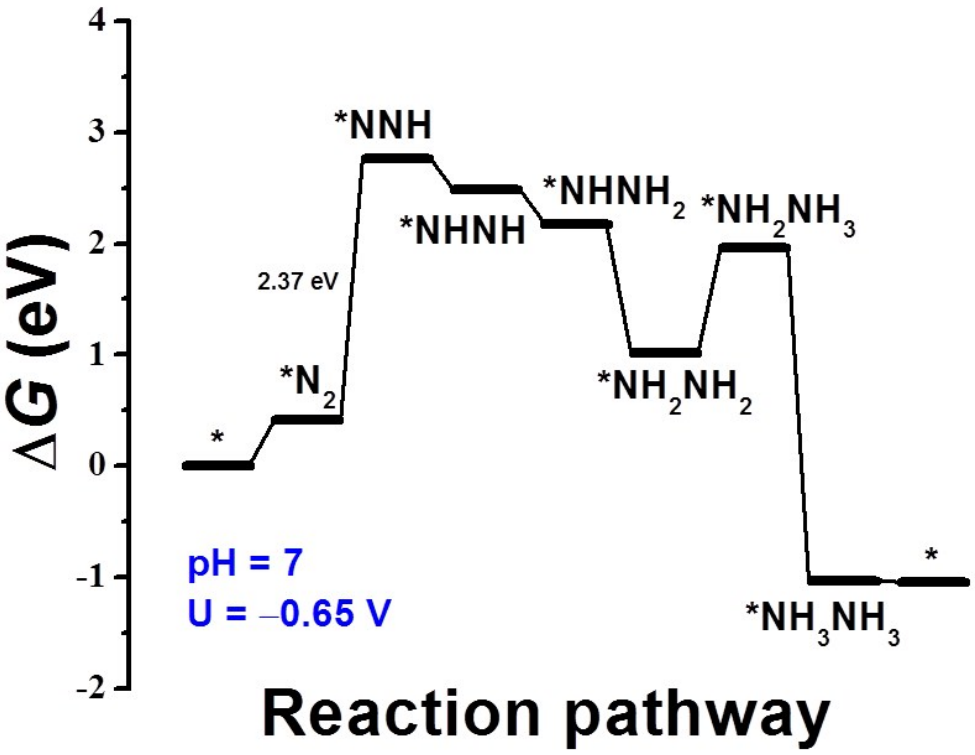

Fig. S12. Free energy diagram on G catalyst for the NRR.

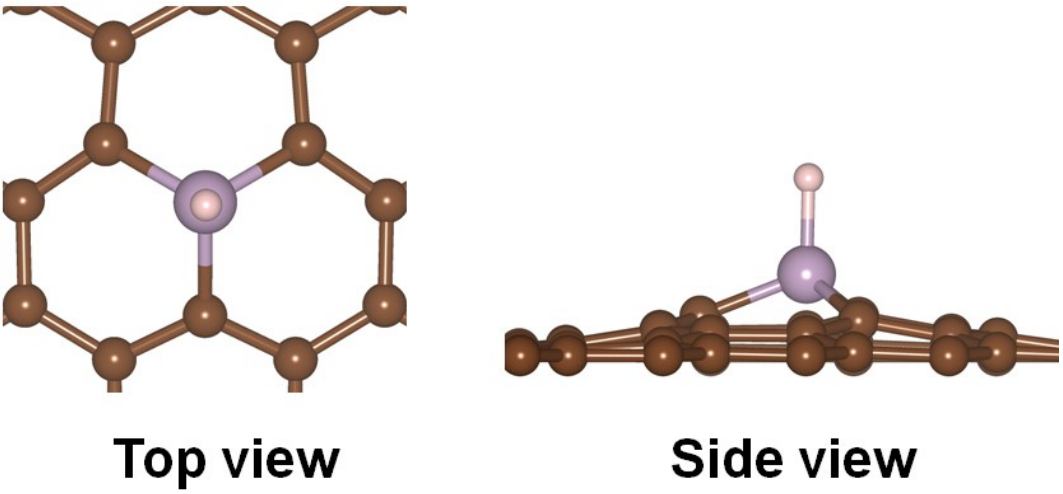

Fig. S13. Free energy change of *H adsorption on PG catalyst and corresponding atom configurations.

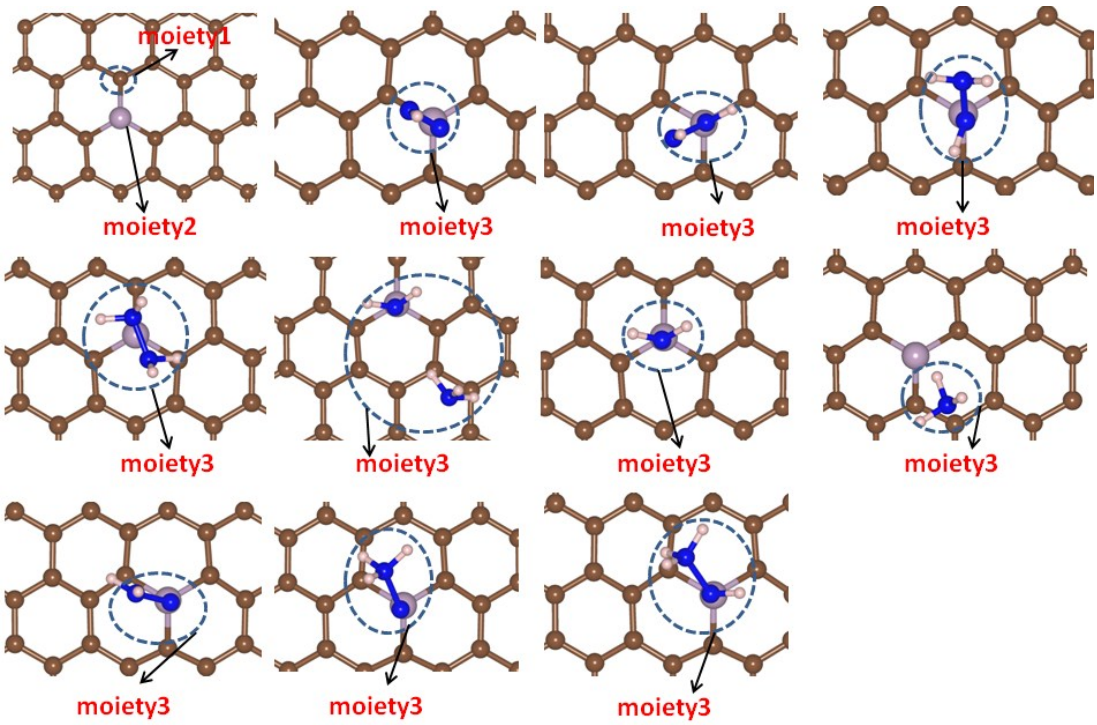

Fig. S14. The three moieties on PG catalyst for NRR.

Table S1. Comparison of the catalytic performances of PG with reported metal-free NRR catalysts at ambient condition.

Catalyst	Electrolyte	NH_3 yield	FE (%)	Ref.
PG	0.5 M $LiClO_4$	32.33 μg h^{-1} $mg^{-1}_{cat.}$	20.82	This work
O-doped graphene	0.1 M HCl	21.3 μg h^{-1} $mg^{-1}_{cat.}$	12.6	12
S-doped graphene	0.1 M HCl	27.3 μg h^{-1} $mg^{-1}_{cat.}$	11.5	13
B-doped graphene	0.05 M H_2SO_4	9.8 μg h^{-1} cm^{-2}	10.8	14
defect-rich fluorographene	0.1 M Na_2SO_4	9.3 μg h^{-1} $mg^{-1}_{cat.}$	4.2	15
defect-rich carbon cloth	0.1 M Na_2SO_4 0.02 M H_2SO_4	15.9 μg h^{-1} cm^{-2}	6.92	16
B_4C	0.1 M HCl	26.57 μg h^{-1} $mg^{-1}_{cat.}$	15.95	17
polymeric carbon nitride	0.1 M HCl	8.09 μg h^{-1} $mg^{-1}_{cat.}$	11.59	18
mesoporous boron nitride	0.1 M Na_2SO_4	18.2 μg h^{-1} $mg^{-1}_{cat.}$	5.5	19
O-doped carbon nanosheet	0.1 M HCl	20.15 μg h^{-1} $mg^{-1}_{cat.}$	4.97	20
O-doped hollow carbon microtubes	0.1 M HCl	25.12 μg h^{-1} $mg^{-1}_{cat.}$	9.1	21
N-doped carbon nanospikes	0.25 M $LiClO_4$	97.18 ± 7.13 μg h^{-1} cm^{-2}	11.56 ± 0.85	22
N-doped highly disordered carbon	0.1 M KOH	57.8 μg h^{-1} cm^{-2}	10.2	23
N-doped porous carbon	0.05 M H_2SO_4	23.8 μg h^{-1} $mg^{-1}_{cat.}$	1.42	24
S-graphene nanohybrid	0.5 M $LiClO_4$	28.56 μg h^{-1} $mg^{-1}_{cat.}$	7.07	25
S-doped carbon nanosphere	0.1 M Na_2SO_4	19.07 μg h^{-1} $mg^{-1}_{cat.}$	7.47	26
N and B co-doped carbon nanosheet	0.1 M HCl	7.75 μg h^{-1} $mg^{-1}_{cat.}$	13.79	27
BP nanoparticle	0.1 M HCl	26.42 μg h^{-1} $mg^{-1}_{cat.}$	12.7	28

oxidized carbon nanotube	0.1 M $LiClO_4$	32.33 μg h^{-1} $mg^{-1}_{cat.}$	12.5	29
hexagonal boron nitride nanosheet	0.1 M HCl	22.4 μg h^{-1} $mg^{-1}_{cat.}$	4.7	30
boron nanosheet	0.1 M Na_2SO_4	13.22 μg h^{-1} $mg^{-1}_{cat.}$	4.04	31
boron nanosheet	0.1 M HCl	3.12 μg h^{-1} $mg^{-1}_{cat.}$	4.84	32

References

1 L. J. Cote, F. Kim and J. Huang, *J. Am. Chem. Soc*., 2009, **131**, 1043–1049.

2 W. S. Hummers and R. E. Offeman, *J. Am. Chem. Soc.*, 1958, **80**, 1339.

3 D. Zhu, L. Zhang, R. E. Ruther and R. J. Hamers, *Nat. Mater.*, 2013, **12**, 836–841.

4 G. W. Watt and J. D. Chrisp, *Anal. Chem.*, 1952, **24**, 2006–2008.

5 G. Kresse and J. Furthmüller, *Comp. Mater. Sci.*, 1996, **6**, 15–50.

6 G. Kresse and J. Furthmüller, *Phys. Rev. B*, 1996, **54**, 11169.

7 J. P. Perdew, K. Burke and M. Ernzerhof, *Phys. Rev. Lett.*, 1996, **77**, 3865–3868.

8 X. Zhang, Z. Lu, Z. Fu, Y. Tang, D. Ma and Z. Yang, *J. Power Sources*, 2015, **276**, 222–229.

9 S. Grimme, J. Antony, S. Ehrlich and H. Krieg, *J. Chem. Phys.*, 2010, **132**, 154104.

10 E. Skulason, G. S. Karlberg, J. Rossmeisl, T. Bligaard, J. Greeley, H. Jonsson and J. K. Nørskov, *Phys. Chem. Chem. Phys.*, 2007, **9**, 3241–3250.

11 https://janaf.nist.gov/.

12 T. Wang, L. Xia, J. Yang, H. Wang, W. Fang, H. Chen, D. Tang, A. M. Asiri, Y. Luo, G. Cui and X. Sun, *Chem. Commun.*, 2019, **55**, 7502–7505.

13 L. Xia, J. Yang, H. Wang, R. Zhao, H. Chen, W. Fang, A. M. Asiri, F. Xie, G. Cui and X. Sun, *Chem. Commun.*, 2019, **55**, 3371–3374.

14 X. Yu, P. Han, Z. Wei, L. Huang, Z. Gu, S. Peng, J. Ma and G. Zheng, *Joule*, 2018, **2**, 1610–1622.

15 J. Zhao, J. Yang, L. Ji, H. Wang, H. Chen, Z. Niu, Q. Liu, T. Li, G. Cui and X. Sun, *Chem. Commun.*, 2019, **55**, 4266–4269.

16 W. Li, T. Wu, S. Zhang, Y. Liu, C. Zhao, G. Liu, G. Wang, H. Zhang and H. Zhao, *Chem. Commun.*, 2018, **54**, 11188–11191.

17 W. Qiu, X. Xie, J. Qiu, W. Fang, R. Liang, X. Ren, X. Ji, G. Cui, A. M. Asiri, G. Cui, B. Tang and X. Sun, *Nat. Commun.*, 2018, **9**, 3485.

18 C. Lv, Y. Qian, C. Yan, Y. Ding, Y. Liu, G. Chen and G. Yu, *Angew. Chem. Int. Ed.*, 2018, **57**, 10246–10250.

19 J. Zhao, X. Ren, X. Li, D. Fan, X. Sun, H. Ma, Q. Wei and D. Wu, *Nanoscale*, 2019, **11**, 4231–4235.

20 H. Huang, L. Xia, R. Cao, Z. Niu, H. Chen, Q. Liu, T. Li, X. Shi, A. M. Asiri and X. Sun, *Chem. Eur. J.*, 2019, **25**, 1914–1917.

21 T. Wu, P. Li, H. Wang, R. Zhao, Q. Zhou, W. Kong, M. Liu, Y. Zhang, X. Sun and F. Gong, *Chem. Commun*., 2019, **55**, 2684–2687.

22 Y. Song, D. Johnson, R. Peng, D. K. Hensley, P. V. Bonnesen, L. Liang, J. Huang, F. Yang, F. Zhang, R. Qiao, A. P. Baddorf, T. J. Tschaplinski, N. L. Engle, M. C. Hatzell, Z. Wu, D. A. Cullen, H. M. Meyer, B. G. Sumpter and A. J. Rondinone, *Sci. Adv.*, 2018, **4**, e1700336.

23 S. Mukherjee, D. A. Cullen, S. Karakalos, K. Liu, H. Zhang, S. Zhao, H. Xu, K. L. More, G. Wang and G. Wu, *Nano Energy*, 2018, **48**, 217–226.

24 Y. Liu, Y. Su, X. Quan, X. Fan, S. Chen, H. Yu, H. Zhao, Y. Zhang and J. Zhao, *ACS Catal.*, 2018, **8**, 1186–1191.

25 H. Chen, X. Zhu, H. Huang, H. Wang, T Wang, R. Zhao, H. Zheng, A. M. Asiri, Y. Luo and X. Sun, *Chem. Commun.*, 2019, **55**, 3152–3155.

26 L. Xia, X. Wu, Y. Wang, Z. Niu, Q. Liu, T. Li, X. Shi, A. M. Asiri and X. Sun, *Small Methods*, 2018, **14**, 1800251.

27 C. Chen, D. Yan, Y. Wang, Y. Zhou, Y. Zou, Y. Li and S. Wang, *Small*, 2019, **15**, 1805029.

28 X. Zhu, T. Wu, L. Ji, L. C. Li, T. Wang, S. Wen, S. Gao, X. Shi, Y. Luo and X. Sun, *J. Mater. Chem. A*, 2019, **7**, 16117–16121.

29 J. Zhao, B. Wang, Q. Zhou, H. Wang, X. Li, H. Chen, Q. Wei, D. Wu, Y. Luo, J. You, F. Gong and X Sun, *Chem. Commun.*, 2019, **55**, 4997–5000.

30 Y. Zhang, H. Du, Y. Ma, L. Ji, H. Guo, Z. Tian, H. Chen, H. Huang, G. Cui, A. M. Asiri, F. Qu, L. Chen and X. Sun, *Nano Res*., 2019, **12**, 919–924.

31 X. Zhang, T. Wu, H. Wang, R. Zhao, H. Chen, T. Wang, P. Wei, Y. Luo, Y. Zhang and X. Sun, *ACS Catal.*, 2019, **9**, 4609–4615.

32 Q. Fan, C. Choi, C. Yan, Y. Liu, J. Qiu, S. Hong, Y. Jung and Z. Sun, *Chem. Commun*., 2019, **55**, 4246–4249.